
Supporting Information

Identifying the Superatomic AuCu₅₆ Nanocluster through a Ligand-exchange Coupled Metal-exchange Induced Transformation

Saniya Gratiious,^a Bo Li,^b Dipanjana Mondal,^c Alok Kumar,^a Dayona Aleyamma Varghese,^a Jibin Thomas,^a De-en Jiang,^{b} Vinayak Kamble,^c Sukhendu Mandal^{a*}*

^aSchool of Chemistry, Indian Institute of Science Education and Research Thiruvananthapuram, Maruthamala P.O., Trivandrum, India-695551. Email: sukhendu@iisertvm.ac.in

^bDepartment of Chemical and Biomolecular Engineering, Vanderbilt University, Nashville, Tennessee 37235, United States
Email: de-en.jiang@vanderbilt.edu

^cSchool of Physics, Indian Institute of Science Education and Research Thiruvananthapuram, Maruthamala P.O., Trivandrum, India-695551.

Table of Contents

Name	Description	Page No.
	Experimental section	S3-S12
Figure S1	UV-vis absorption and MALDI-MS spectra of the synthesized $[\text{Au}_{23}(\text{S}-c\text{-C}_6\text{H}_{11})_{16}]^- \text{NC}$	S13
Figure S2	Time-dependent UV-vis absorption spectra during the transformation of $[\text{Au}_{23}(\text{S}-c\text{-C}_6\text{H}_{11})_{16}]^- \text{NC}$	S14
Figure S3	Time-dependent MALDI-TOF mass spectra during the transformation of $[\text{Au}_{23}(\text{S}-c\text{-C}_6\text{H}_{11})_{16}]^- \text{NC}$ before addition of Cu(I) salt	S15
Table S1	Table showing the formula corresponding to peaks from Fig. S3	S15
Figure S4	Time-dependent MALDI-TOF mass spectra during the transformation of $[\text{Au}_{23}(\text{S}-c\text{-C}_6\text{H}_{11})_{16}]^- \text{NC}$ after adding Cu(I) salt	S16
Figure S5	Positive-ion mode ESI-MS spectrum of the aliquot taken during the transformation of $[\text{Au}_{23}(\text{S}-c\text{-C}_6\text{H}_{11})_{16}]^- \text{NC}$	S16
Figure S6	Optical microscope image of the single crystals of $\text{AuCu}_{56} \text{NC}$	S17
Table S2	Crystal structure parameters of $\text{AuCu}_{56} \text{NC}$	S18
Table S3	Selected bond distances observed in $\text{AuCu}_{56} \text{NC}$	S19-S20
Figure S7	The innermost Cu_{14} rhombic dodecahedron of the $[\text{AuCu}_{56}\text{S}_{12}(\text{AdmS})_{20}(\text{O}_3\text{SAdm})_{12}] \text{NC}$	S21
Figure S8	The unit cell packing of the $\text{AuCu}_{56} \text{NC}$	S21
Figure S9	The intermolecular interactions of the $\text{AuCu}_{56} \text{NC}$	S22
Figure S10	The TEM image of the $\text{AuCu}_{56} \text{NC}$ and b) the bar diagram showing the average size of the particles	S23
Figure S11	The TEM elemental analysis showing the composition of the $\text{AuCu}_{56} \text{NC}$	S24
Figure S12	XPS spectra of $\text{AuCu}_{56} \text{NC}$ (a) S 2p orbitals, and b) survey spectrum	S25
Figure S13	Cyclic and differential pulse voltammograms of $\text{AuCu}_{56} \text{NC}$	S26
Table S4	Experimental formal potential differences for $\text{AuCu}_{56} \text{NC}$	S26
Figure S14	Differential pulse voltammograms and cyclic voltammograms at 10 mV/s of $\text{AuCu}_{56} \text{NC}$. Schematic representation of the energy level diagram for $\text{AuCu}_{56} \text{NC}$.	S27
Figure S15	EPR spectrum of the $\text{AuCu}_{56} \text{NC}$	S27
Figure S16	Concentric bond analysis of the core structure $\text{Au}@\text{Cu}_{14}\text{S}_{12}@\text{Cu}_{36}$ extracted from the optimized geometry of the AuCu_{56} cluster: a) HOMO; b) contour plot of the HOMO projected along the 6-fold axis of the $[\text{Cu}_{14}]$ rhombic dodecahedron.	S28
Figure S17	Optical microscopic image of the drop-casted AuCu_{56} device and the response and recovery times	S29
Figure S18	Photoresponse of the device made of $\text{AuCu}_{56} \text{NC}$ under white light irradiation	S30
	References	S30

I. Experimental Section

1.1. Materials

All chemicals were purchased commercially and used without prior purification. Tetrachloroauric (III) acid ($\text{HAuCl}_4 \cdot 3\text{H}_2\text{O}$, > 99.9% metals basis), tetraoctylammonium bromide (TOAB, $\geq 98\%$), cyclohexane thiol (*S-c-C*₆H₁₁; 97%), sodium borohydride (NaBH_4 , 99.99%, trace metal basis), Tetrakis(acetonitrile)copper(I) tetrafluoroborate ($\text{Cu}(\text{ACN})_4(\text{BF}_4)$, 97%), 1-adamantanethiol ($\text{C}_{10}\text{H}_{15}\text{SH}$, 95%), trans-2-[3-(4-*tert*-butylphenyl)-2-methyl-2-propenylidene] malononitrile (DCTB, > 99.0%) were purchased from Sigma-Aldrich. MeOH (HPLC grade, 99.9%, Spectrochem), dimethylene chloride (DCM, HPLC grade, 99.9%, Spectrochem), and acetonitrile (ACN, HPLC grade, 99.9%), were used as purchased. The water used in all experiments was ultrapure (resistivity: 18.2 M Ω cm), produced by a Milli-Q NANO pure water system. All glassware was thoroughly cleaned with aqua regia ($\text{HCl}:\text{HNO}_3 = 3:1$, v: v) and rinsed with abundant pure water.

1.2. Methods

Synthesis of $[\text{Au}_{23}(\text{S-c-C}_6\text{H}_{11})_{16}]^-$ nanocluster. The $[\text{Au}_{23}(\text{S-c-C}_6\text{H}_{11})_{16}]^-$ nanocluster (NC) was synthesized by following the previously reported method.^{S1} The $\text{HAuCl}_4 \cdot 3\text{H}_2\text{O}$ (0.6 mmol, 236.3 mg) was dissolved in 30 mL of methanol in a 50 mL tri-necked round-bottom flask, to which the tetraoctylammonium bromide (TOAB, 0.696 mmol, 380 mg) was added. This solution upon stirring for 15 min was treated with 1-cyclohexanethiol (3.2 mmol, 390 μL) at room temperature. The solution turned yellowish cloudy from reddish brown almost immediately. After 15 min, freshly prepared NaBH_4 (6 mmol, 227 mg) dissolved in 12 mL of cold nano pure water was rapidly added to the solution under vigorous stirring. The solution turned blackish immediately, indicating the formation of Au NCs, which gradually precipitated out of the MeOH solvent. This solution was then stirred overnight and further washed with MeOH several times to remove excess thiol and yield pure $[\text{Au}_{23}(\text{S-c-C}_6\text{H}_{11})_{16}]^-$ NC (~ 20% yield, Au-atom basis).

Synthesis of $[\text{AuCu}_{56}\text{S}_{12}(\text{AdmS})_{20}(\text{O}_3\text{SAdm})_{12}]$ nanocluster: 7.5 mg of $[\text{Au}_{23}(\text{S-c-C}_6\text{H}_{11})_{16}]^-$ was dissolved in 5 mL of dichloromethane and was centrifuged at (25 °C, 8000 rpm) for 10 minutes to remove any insoluble particles. 150 mg of 1-adamantanethiol was added to this solution followed

by 50 mg of Tetrakis(acetonitrile)copper(I) tetrafluoroborate dissolved in 1.5 mL ACN. This reaction mixture was stirred for 2 h at room temperature. This reaction mixture was then rotavapped to dryness, washed several times with MeOH and ACN to remove excess reagents and extracted using DCM. Single crystals of the as-prepared NCs were grown at room temperature by layering the DCM solution of the clusters with hexane in three weeks. (~10% yield, Cu-atom basis).

II. Characterization procedures

The absorption spectra were obtained on a UV-3800 SHIMADZU UV-Vis NIR spectrometer using dichloromethane as a solvent. The mass spectra of the transformed products were acquired by using a Bruker Microflex MALDI-TOF mass spectrometer. DCTB was used as a matrix and the sample was prepared as 1 mg in 100 μ L of dichloromethane. From the stock solution, various amounts of the stock solution were taken and mixed with 1 μ L of the analyte solution. The molecules were ionized with the Nd: YAG laser ($\lambda = 266$ nm). The analyte concentration was optimized to get a well-resolved spectrum. ESI mass spectra were recorded using a Waters Q-TOF mass spectrometer equipped with a Z-Spray source. The source temperature was kept at 90 $^{\circ}$ C. The sample was directly infused into the chamber at 5 μ L/min. The spray voltage was kept at 3.5 kV and the cone voltage at 30 V. To prepare the ESI sample, clusters were dissolved in dichloromethane (1 mg/ mL) and diluted (2: 1 v) using methanol solvent. Optical microscope image of the AuCu₅₆NC was taken on Leica microscope equipped with an MC170 HD camera. FEI Tecnai G2 F30 STwin transmission electron microscope (TEM) 300 kV, scanning electron microscope (SEM), and energy-dispersive X-ray spectroscopy (EDS; FEI Nova NANOSEM 450) were used for the microscopic characterization. X-ray photoelectron spectroscopy (XPS) measurements were performed using the Omicron Nanotech instrument with a Mg K α X-ray source, casaXPS software was used for data analysis. The carbon correction with respect to 284.8 eV was done for all the elements. Electron paramagnetic resonance (EPR) spectrum was recorded on powder sample using JEOL JES-X320 EPR spectrometer at 298 K.

2.1 Single Crystal X-Ray Diffraction

The single crystal of [AuCu₅₆S₁₂(AdmS)₂₀(O₃SAdm)₁₂] with dimensions of 0.130 mm \times 0.150 mm \times 0.160 mm was mounted on Bruker D8 Quest - Microfocus SCXRD (single crystal X-ray diffractometer) with Bruker PHOTON III C14, CPAD detector using MoK α radiation ($\lambda = 0.71073$ Å). The total exposure time for data collection was 1.87 hours. The frames were integrated with

the Bruker SAINTS software package using a narrow-frame algorithm. The crystal structure was solved using the charge-flipping algorithm, as implemented in the program SUPERFLIP² and refined by full-matrix least-squares techniques against F_o^2 using the SHELXL program^{3,4} through the OLEX2 interface.⁵ Hydrogen atoms on the surface were placed in calculated positions and refined isotropically by using a riding model. Appropriate restraints or constraints were applied to the geometry and the atomic displacement parameters of the atoms in the AuCu₅₆ nanocluster. The crystal structure refinement parameters of the AuCu₅₆ nanocluster is given in Table S2.

Refinement model description

Number of restraints - 2070, number of constraints - unknown.

Details:

1. Restrained distances

C01F-C00Z

2.5 with sigma of 0.001

C02E-C026 = C026-C012 = C028-C012 = C21-C02E = C21-C021 = C028-C021 = C021-

C01V = C01S-C012 = C01S-C01R = C02E-C024 = C01V-C01R = C024-C01R

1.55 with sigma of 0.001

C1E-C1D = C1F-C1E = C21A-C1F = C1D-C01W = C1C-C01W = C21A-C1C = C26-C1C = C1H-

C1D = C1H-C012 = C1G-C1F = C1G-C012 = C26-C012

1.55 with sigma of 0.001

C02E-C01R

2.5 with sigma of 0.001

C01R-C021

2.5 with sigma of 0.001

C1G-C1E

2.5 with sigma of 0.001

C1E-C1H

2.5 with sigma of 0.001

C01K-C01O

2.5 with sigma of 0.001

C025-C010 = C027-C010 = C01I-C010 = C01U-C01I = C1-C027 = C025-C01D = C4-C01U

= C01U-C01C = C1-C01C = C62-C1 = C62-C01D = C4-C01D

1.55 with sigma of 0.001

C01Q-C015 = C14-C015 = C14-C10 = C02F-C015 = C16-C02F = C20-C16 = C20-C10 =

C02G-C01Q = C17-C02G

1.55 with sigma of 0.001

C01V-C21

2.5 with sigma of 0.001

C01J-C01F

2.5 with sigma of 0.001

C024-C01V

2.5 with sigma of 0.001

C02F-C01Q

2.5 with sigma of 0.001

C021-C02E

2.5 with sigma of 0.001

C023-C01Z

1.55 with sigma of 0.001

C21-C024

2.5 with sigma of 0.001

C02A-C01K
2.5 with sigma of 0.001
C01Q-C11
2.5 with sigma of 0.001
C01Z-C00Z
2.5 with sigma of 0.001
C01J-C01Z
2.5 with sigma of 0.001
C023-C02A
2.5 with sigma of 0.001
C01K-C023
2.5 with sigma of 0.001
C00Z-C01J
2.5 with sigma of 0.001
C2-C25
2.5 with sigma of 0.001
C17-C10
1.55 with sigma of 0.001
C11-C16
1.55 with sigma of 0.001
C11-C02G
1.55 with sigma of 0.001
C015-C02G
2.5 with sigma of 0.001
C16-C015
2.5 with sigma of 0.001
C11-C02F
2.5 with sigma of 0.001
C02G-C16
2.5 with sigma of 0.001
C14-C02F
2.5 with sigma of 0.001
C10-C015
2.5 with sigma of 0.001
C16-C10
2.5 with sigma of 0.001
C20-C14
2.5 with sigma of 0.001
C015-C10
2.5 with sigma of 0.001
C02F-C20
2.5 with sigma of 0.001
C24-C01X
2.5 with sigma of 0.001
C01X-C01T
2.5 with sigma of 0.001
C01T-C24
2.5 with sigma of 0.001
C2-C01T
1.55 with sigma of 0.001
C62A-C01E
1.55 with sigma of 0.001
C19-C015 = C14A-C015 = C15-C015
1.55 with sigma of 0.001
C17A-C02H = C17A-C10A = C20A-C10A = C20A-C16A = C16A-C11A = C11A-C02H
1.55 with sigma of 0.001

C11A-C15
2.5 with sigma of 0.001
C19-C11A
2.5 with sigma of 0.001
C16A-C015
2.5 with sigma of 0.001
C16A-C02H
2.5 with sigma of 0.001
C15-C19
2.5 with sigma of 0.001
C02H-C015
2.5 with sigma of 0.001
C15-C10A
2.94 with sigma of 0.001
C6A-C00Z = C02B-C00Z = C02B-C01{ = C01L-C00Z = C23-C01L = C1B-C01{ = C01P-
C01G = C6A-C01G = C7A-C01{ = C23-C01P = C7A-C01G = C23-C1B
1.55 with sigma of 0.001
C02B-C7A
2.5 with sigma of 0.001
C00Z-C01{
2.5 with sigma of 0.001
C6A-C02B
2.5 with sigma of 0.001
C01{-C01G
2.5 with sigma of 0.001
C7A-C6A
2.5 with sigma of 0.001
C01G-C00Z
2.5 with sigma of 0.001
C01W-C26
2.5 with sigma of 0.001
C1D-C1C
2.5 with sigma of 0.001
C1H-C01W
2.5 with sigma of 0.001
C012-C1D
2.5 with sigma of 0.001
C26-C1H
2.5 with sigma of 0.001
C1C-C012
2.5 with sigma of 0.001
C012-C1F
2.5 with sigma of 0.001
C1H-C1G
2.5 with sigma of 0.001
C1D-C012
2.5 with sigma of 0.001
C1F-C1D
2.5 with sigma of 0.001
C3A-C25A = C3A-C22A = C25A-C24A = C2A-C24A = C2A-C18A = C2A-C1I = C5-C27 = C5-
C01Y = C25A-C01Y = C27-C22A = C22A-C18A = C5-C1I
1.55 with sigma of 0.001
C2A-C22A
2.5 with sigma of 0.001
C5-C2A
2.5 with sigma of 0.001

C18A-C27
 2.5 with sigma of 0.001
 C11-C18A
 2.5 with sigma of 0.001
 C27-C11
 2.5 with sigma of 0.001
 C5-C25A
 2.5 with sigma of 0.001
 C27-C01Y
 2.5 with sigma of 0.001
 C22A-C5
 2.5 with sigma of 0.001
 C25A-C22A
 2.5 with sigma of 0.001
 C3A-C27
 2.5 with sigma of 0.001
 C01Y-C3A
 2.5 with sigma of 0.001
 2. Uiso/Uanisotropic restraints and constraints
 S6 ≈ C012 ≈ C01R ≈ C01S ≈ C01V ≈ C021 ≈ C024 ≈ C026
 ≈ C028 ≈ C02E ≈ C21 ≈ C26 ≈ C1C ≈ C01W ≈ C1D ≈
 C1E ≈ C21A ≈ C1F ≈ C1G ≈ C1H: within 2A with sigma of 0.004 and
 sigma for terminal atoms of 0.008 within 2A
 Cu7 ≈ Cu8 ≈ Cu5B: within 2A with sigma of 0.004 and sigma for terminal
 atoms of 0.008 within 2A
 Cu1A ≈ Cu1B: within 2A with sigma of 0.004 and sigma for terminal atoms of
 0.008 within 2A
 S3 ≈ O00W ≈ C00Z ≈ O016 ≈ C01J ≈ C01K ≈ C01Z ≈ C023
 ≈ C02A ≈ O37 ≈ O00X ≈ O2 ≈ C6 ≈ C7 ≈ O37A ≈
 C01F ≈ C01O: within 2A with sigma of 0.004 and sigma for terminal atoms of
 0.008 within 2A
 Cu2A ≈ Cu2 ≈ Cu2B: within 2A with sigma of 0.004 and sigma for terminal
 atoms of 0.008 within 2A
 S1 ≈ C ≈ C00Y ≈ C00X ≈ C011: within 2A with sigma of 0.004 and
 sigma for terminal atoms of 0.008 within 2A
 Cu1A ≈ Cu1 ≈ Cu1B: within 2A with sigma of 0.004 and sigma for terminal
 atoms of 0.008 within 2A
 Cu3A ≈ Cu3: within 2A with sigma of 0.004 and sigma for terminal atoms of
 0.008 within 2A
 S4 ≈ C010 ≈ C01C ≈ C01D ≈ C01I ≈ C01U ≈ C025 ≈ C027
 ≈ C1 ≈ C4 ≈ C62 ≈ C8 ≈ C0 ≈ C1A ≈ C9 ≈ C12
 ≈ C62A ≈ C4A ≈ C01E ≈ C13: within 2A with sigma of 0.004 and
 sigma for terminal atoms of 0.008 within 2A
 C015 ≈ C01Q ≈ C02F ≈ C02G ≈ C10 ≈ C11 ≈ C14 ≈ C16
 ≈ C20 ≈ C17 ≈ C14A ≈ C15 ≈ C17A ≈ C10A ≈ C20A ≈
 C11A ≈ C02H ≈ C19 ≈ C16A ≈ S8 ≈ O017 ≈ O018 ≈ O01H
 ≈ O0 ≈ O01I ≈ O1: within 2A with sigma of 0.004 and sigma for
 terminal atoms of 0.008 within 2A
 C00Z ≈ C01F ≈ C01J ≈ C01K ≈ C01O ≈ C01Z ≈ C023 ≈
 C02A ≈ C6 ≈ C7 ≈ C01L ≈ C23 ≈ C1B ≈ C01 { ≈ C02B
 ≈ C7A ≈ C01G ≈ C6A ≈ C01P ≈ S3 ≈ O00W ≈ O016 ≈
 O37A ≈ O2 ≈ O37 ≈ O00X: within 2A with sigma of 0.004 and sigma for
 terminal atoms of 0.008 within 2A
 S5 ≈ C019 ≈ C01T ≈ C01X ≈ C2 ≈ C24 ≈ C25 ≈ C18
 ≈ C3 ≈ C22 ≈ C5 ≈ C27 ≈ C01Y ≈ C1I ≈ C25A ≈ C3A
 ≈ C22A ≈ C18A ≈ C2A ≈ C24A: within 2A with sigma of 0.004 and

sigma for terminal atoms of 0.008 within 2A
 Cu10 ≈ Cu11: within 2A with sigma of 0.004 and sigma for terminal atoms of 0.008 within 2A
 Cu11 ≈ Cu10: within 2A with sigma of 0.004 and sigma for terminal atoms of 0.008 within 2A
 Cu13 ≈ Cu20 ≈ Cu17 ≈ Cu21 ≈ Cu16: within 2A with sigma of 0.004 and sigma for terminal atoms of 0.008 within 2A
 Cu15 ≈ Cu18 ≈ Cu12 ≈ Cu21: within 2A with sigma of 0.004 and sigma for terminal atoms of 0.008 within 2A

3. Others

1*[Sof(Cu2B)]+1*[Sof(Cu2A)]+1*[Sof(Cu2)]=1 with esd of 0
 1*[Sof(Cu5B)]+1*[Sof(Cu5)]+1*[Sof(Cu5A)]=1 with esd of 0
 1*[Sof(Cu1B)]+1*[Sof(Cu1A)]+1*[Sof(Cu1)]=1 with esd of 0
 1*[Sof(Cu16)]+1*[Sof(Cu20)]+1*[Sof(Cu21)]+1*[Sof(Cu17)]+1*[Sof(Cu13)]=1 with esd of 0
 1*[Sof(Cu14)]+1*[Sof(Cu12)]+1*[Sof(Cu18)]+1*[Sof(Cu15)]=1 with esd of 0
 Sof(Cu4A)=1-FVAR(1)
 Sof(Cu4)=FVAR(1)
 Sof(Cu6)=1-FVAR(5)
 Sof(Cu6A)=FVAR(5)
 Sof(Cu3)=1-FVAR(6)
 Sof(Cu3A)=FVAR(6)
 Sof(O0)=Sof(O01I)=Sof(O1)=1-FVAR(13)
 Sof(O017)=Sof(O018)=Sof(O01H)=FVAR(13)
 Sof(O00X)=Sof(O37A)=Sof(O2)=1-FVAR(14)
 Sof(O00W)=Sof(O016)=Sof(O37)=FVAR(14)
 Sof(C8)=Sof(H8A)=Sof(H8B)=Sof(C0)=Sof(H0A)=Sof(H0B)=Sof(C1A)=Sof(H1A)=Sof(C9)=
 Sof(H9A)=Sof(H9B)=Sof(C12)=Sof(H12)=Sof(C62A)=Sof(H62C)=Sof(H62D)=Sof(C4A)=
 Sof(H4AA)=Sof(H4AB)=Sof(C01E)=Sof(H3)=Sof(C13)=Sof(H13A)=Sof(H13B)=1-FVAR(15)
 Sof(C01C)=Sof(H01E)=Sof(H01F)=Sof(C01D)=Sof(H01G)=Sof(C01I)=Sof(H01I)=
 Sof(H01J)=Sof(C01U)=Sof(H01W)=Sof(C025)=Sof(H02E)=Sof(H02F)=Sof(C027)=
 Sof(H02I)=Sof(H02J)=Sof(C1)=Sof(H1)=Sof(C4)=Sof(H4A)=Sof(H4B)=Sof(C62)=
 Sof(H62A)=Sof(H62B)=FVAR(15)
 Sof(C14A)=Sof(H14C)=Sof(H14D)=Sof(C15)=Sof(H15A)=Sof(H15B)=Sof(C17A)=
 Sof(H17C)=Sof(H17D)=Sof(C10A)=Sof(H10A)=Sof(C20A)=Sof(H20C)=Sof(H20D)=
 Sof(C11A)=Sof(H11C)=Sof(H11D)=Sof(C02H)=Sof(H02S)=Sof(C19)=Sof(H19A)=Sof(H19B)=
 Sof(C16A)=Sof(H16A)=1-FVAR(16)
 Sof(C01Q)=Sof(H01P)=Sof(H01Q)=Sof(C02F)=Sof(H02P)=Sof(H02Q)=Sof(C02G)=
 Sof(H02R)=Sof(C10)=Sof(H10)=Sof(C11)=Sof(H11A)=Sof(H11B)=Sof(C14)=Sof(H14A)=
 Sof(H14B)=Sof(C16)=Sof(H16)=Sof(C20)=Sof(H20A)=Sof(H20B)=Sof(C17)=Sof(H17A)=
 Sof(H17B)=FVAR(16)
 Sof(C01L)=Sof(H4)=Sof(HA)=Sof(C23)=Sof(H23)=Sof(C1B)=Sof(H1BA)=Sof(H1BB)=
 Sof(C01{)=Sof(H01{)=Sof(C02B)=Sof(H02T)=Sof(H02U)=Sof(C7A)=Sof(H7AA)=Sof(H7AB)=
 Sof(C01G)=Sof(H5)=Sof(C6A)=Sof(H6AA)=Sof(H6AB)=Sof(C01P)=Sof(H6)=Sof(HB)=1-
 FVAR(17)
 Sof(C01F)=Sof(H01H)=Sof(C01J)=Sof(H01K)=Sof(C01K)=Sof(H01L)=Sof(H01M)=
 Sof(C01O)=Sof(H01N)=Sof(H01O)=Sof(C01Z)=Sof(H01)=Sof(C023)=Sof(H02A)=Sof(H02B)=
 Sof(C02A)=Sof(H02M)=Sof(H02N)=Sof(C6)=Sof(H6A)=Sof(H6B)=Sof(C7)=Sof(H7A)=
 Sof(H7B)=FVAR(17)
 Sof(C26)=Sof(H26A)=Sof(H26B)=Sof(C1C)=Sof(H1C)=Sof(C01W)=Sof(H7)=Sof(HC)=
 Sof(C1D)=Sof(H1D)=Sof(C1E)=Sof(H1EA)=Sof(H1EB)=Sof(C21A)=Sof(H21C)=Sof(H21D)=
 Sof(C1F)=Sof(H1F)=Sof(C1G)=Sof(H1GA)=Sof(H1GB)=Sof(C1H)=Sof(H1HA)=Sof(H1HB)=1-
 FVAR(18)
 Sof(C01R)=Sof(H01R)=Sof(C01S)=Sof(H01S)=Sof(H01T)=Sof(C01V)=Sof(H01X)=
 Sof(H01Y)=Sof(C021)=Sof(H021)=Sof(C024)=Sof(H02C)=Sof(H02D)=Sof(C026)=
 Sof(H02G)=Sof(H02H)=Sof(C028)=Sof(H02K)=Sof(H02L)=Sof(C02E)=Sof(H02O)=Sof(C21)=

Sof(H21A)=Sof(H21B)=FVAR(18)
Sof(C27)=Sof(H27A)=Sof(H27B)=Sof(C01Y)=Sof(H8)=Sof(HD)=Sof(C1I)=Sof(H1IA)=
Sof(H1IB)=Sof(C25A)=Sof(H25A)=Sof(C3A)=Sof(H3AA)=Sof(H3AB)=Sof(C22A)=Sof(H22A)=
Sof(C18A)=Sof(H18C)=Sof(H18D)=Sof(C2A)=Sof(H2A)=Sof(C24A)=Sof(H24C)=Sof(H24D)=
1-FVAR(19)
Sof(C019)=Sof(H01C)=Sof(H01D)=Sof(C01T)=Sof(H01U)=Sof(H01V)=Sof(C01X)=
Sof(H01Z)=Sof(H)=Sof(C2)=Sof(H2)=Sof(C24)=Sof(H24A)=Sof(H24B)=Sof(C25)=
Sof(H25)=Sof(C18)=Sof(H18A)=Sof(H18B)=Sof(C3)=Sof(H3A)=Sof(H3B)=Sof(C22)=
Sof(H22)=FVAR(19)
Fixed Sof: Cu8(0.3333) Cu7(0.3333) Cu9(0.3333) Cu10(0.166667) Cu11(0.1667)
Fixed X: C1E(0.38992)
Fixed Y: C1E(0.79127)
Fixed Z: C1E(0.56754)

4. a Ternary CH refined with riding coordinates:

C00X(H00X), C01D(H01G), C01F(H01H), C01J(H01K), C01R(H01R), C01U(H01W),
C01Z(H01), C021(H021), C02E(H02O), C02G(H02R), C10(H10), C16(H16), C1(H1),
C2(H2), C25(H25), C22(H22), C1A(H1A), C12(H12), C01E(H3), C10A(H10A),
C02H(H02S), C16A(H16A), C23(H23), C01{(H01{)}, C01G(H5), C1C(H1C), C1D(H1D),
C1F(H1F), C25A(H25A), C22A(H22A), C2A(H2A)

4. b Secondary CH2 refined with riding coordinates:

C00Y(H00A,H00B), C011(H01A,H01B), C019(H01C,H01D), C01C(H01E,H01F), C01I(H01I,
H01J), C01K(H01L,H01M), C01O(H01N,H01O), C01Q(H01P,H01Q), C01S(H01S,H01T),
C01T(H01U,H01V), C01V(H01X,H01Y), C01X(H01Z,H), C023(H02A,H02B), C024(H02C,
H02D), C025(H02E,H02F), C026(H02G,H02H), C027(H02I,H02J), C028(H02K,H02L),
C02A(H02M,H02N), C02F(H02P,H02Q), C11(H11A,H11B), C14(H14A,H14B), C20(H20A,
H20B), C17(H17A,H17B), C21(H21A,H21B), C24(H24A,H24B), C18(H18A,H18B), C3(H3A,
H3B), C4(H4A,H4B), C62(H62A,H62B), C6(H6A,H6B), C7(H7A,H7B), C8(H8A,H8B),
C0(H0A,H0B), C9(H9A,H9B), C62A(H62C,H62D), C4A(H4AA,H4AB), C13(H13A,H13B),
C14A(H14C,H14D), C15(H15A,H15B), C17A(H17C,H17D), C20A(H20C,H20D), C11A(H11C,
H11D), C19(H19A,H19B), C01L(H4,HA), C1B(H1BA,H1BB), C02B(H02T,H02U), C7A(H7AA,
H7AB), C6A(H6AA,H6AB), C01P(H6,HB), C26(H26A,H26B), C01W(H7,HC), C1E(H1EA,
H1EB), C21A(H21C,H21D), C1G(H1GA,H1GB), C1H(H1HA,H1HB), C27(H27A,H27B),
C01Y(H8,HD), C1I(H1IA,H1IB), C3A(H3AA,H3AB), C18A(H18C,H18D), C24A(H24C,H24D)

2.2 Electrochemical measurements

Voltammetric measurements were performed using a pine WaveDriver 200 DC Bipotentiostat/Galvanostat Electrochemical workstation. A glassy carbon rotating disk electrode (RDE) (15 mm in diameter) served as the working electrode, while a silver/silver chloride wire and a platinum coil functioned as the quasi-reference and counter electrodes, respectively. Before utilization, the working electrode was polished with 0.05 μm , 0.5 μm , and 1.0- μm Al_2O_3 slurries, followed by cleansing through sonication in isopropanol and water in succession. The electrolyte solution was degassed with ultrahigh-purity nitrogen for a minimum of 20 minutes and maintained under a nitrogen atmosphere throughout the entire experimental process. The working electrode was prepared by drying the NC crystal under vacuum and fine powder was made with the help of a mortar and pestle. A 2 mg powder (NC) was dispersed in 0.5 mL ethanol and a 5 μL Nafion binder was added. The solution was allowed for ultrasonication for 30 min. The prepared well-

dispersed solution was dropcast over GC and air-dried for 5 h. The prepared electrode was used as a working electrode throughout the experiment.

III. Photocurrent studies

3.1 Device fabrication

The Interdigitated electrodes (IDE) devices were fabricated using photolithography technique on a Si/SiO₂ wafer for patterning the design, followed by metal deposition using thermal evaporation. Firstly, a positive photoresist (PR) was spin-coated onto the substrate at 5000 rpm for 40 s. Then, the PR was solidified at 110 °C on a hot plate for 2 min, followed by the exposure of the electrode patterns. After the development process, thermal evaporation was utilized to deposit Cr/Au of 20/80 nm thickness, followed by the lift-off process. The channel length and channel width of the electrodes are kept 100 μm each. For preparing the NC solution 1 mg of the NC was first dispersed in 2 μL ethanol using an ultra-sonic bath for 5 min and then dropcasted on the IDE electrodes. Fig. S16a shows the optical image of the final device.

3.2 Photocurrent measurement

All electrical measurements were performed at room temperature in a two-electrode system Linkam stage with a glass window on the top for light illumination. The electrical responses were recorded using Keithley 2500B multimeter unit. Photodetection experiment was conducted using PSU-H-FDA laser source of 360 nm wavelength and 10 mW power. The device was sourced at a constant bias voltage, and the current with time was recorded for further analysis of the photodetection performance.

IV. Computational details

Spin-polarized density functional theory (DFT) calculations were performed in the Quickstep module of CP2K. The mixed Gaussian and plane wave (GPW) approach using the Perdew-Burke-Ernzerhof (PBE) functional was employed with the Grimme D3-dispersion correction. The Kohn-Sham orbitals were expanded in the molecularly optimized basis set with a double- ζ Gaussian basis set augmented with a set of p-type polarization functions (MOLOPT-SR-DZVP) with core electrons represented by the Goedecker-Teter-Hutter pseudopotentials. In all calculations, the plane-wave kinetic energy cutoff was set to 400 Ry. The convergence threshold of the electronic

structure relaxation was set to 10^{-6} Hartree and the force convergence criterion of the geometry optimizations was set to 4.5×10^{-4} Hartree/Bohr. The computational model of $[\text{AuCu}_{56}\text{S}_{12}(\text{SCH}_3)_{20}(\text{O}_3\text{SCH}_3)_{12}]$ was constructed from the single-crystal structure of $[\text{AuCu}_{56}\text{S}_{12}(\text{AdmS})_{20}(\text{O}_3\text{SAdm})_{12}]$ by replacing the adamantane moieties as methyl groups for the consideration of computation cost. The HOMO, LUMO, and spin density were calculated based on the optimized geometry of $[\text{AuCu}_{56}\text{S}_{12}(\text{SCH}_3)_{20}(\text{O}_3\text{SCH}_3)_{12}]$.

V. Supporting Experimental Data

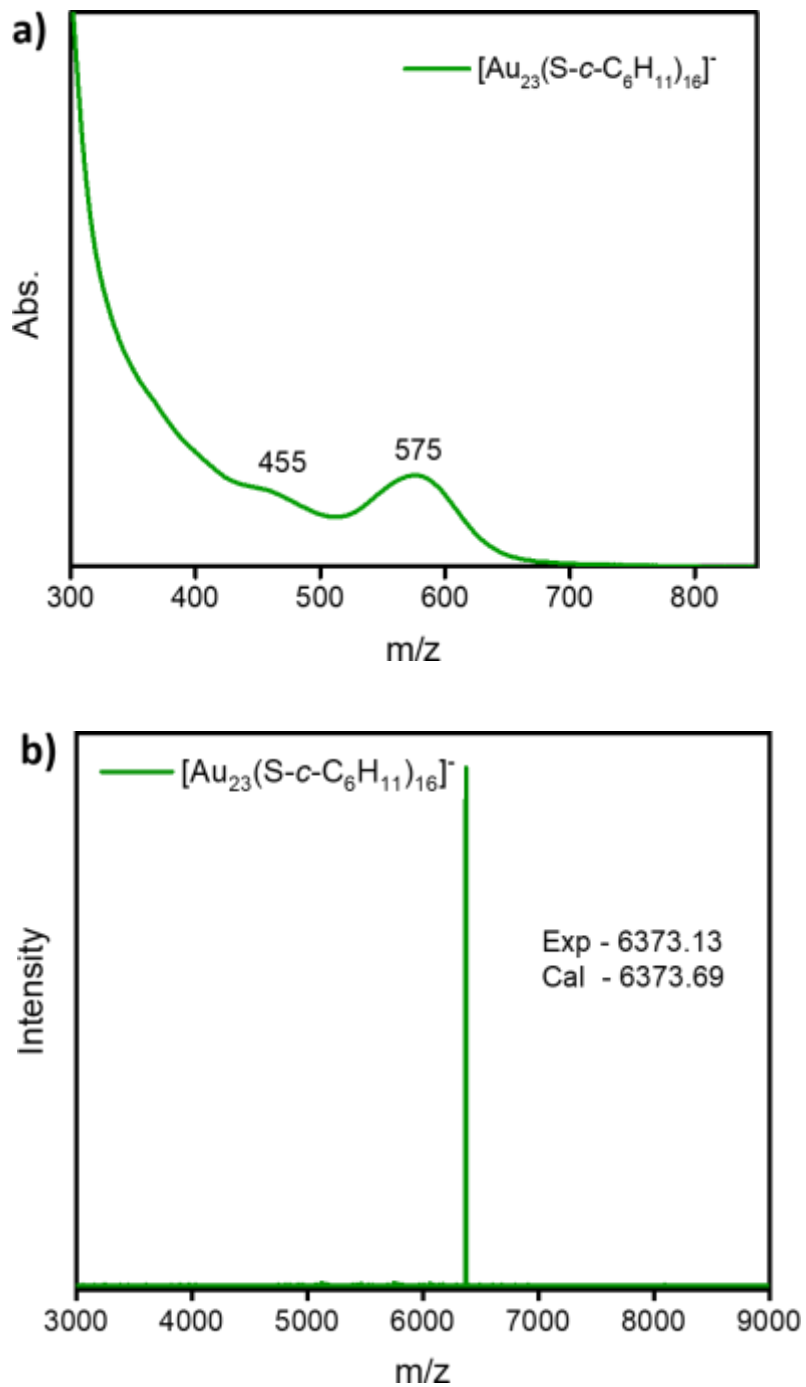


Figure S1. a) UV-vis absorption spectrum and b) MALDI-MS spectrum of the synthesized $[\text{Au}_{23}(\text{S-c-C}_6\text{H}_{11})_{16}]^-$ NC.^{S1}

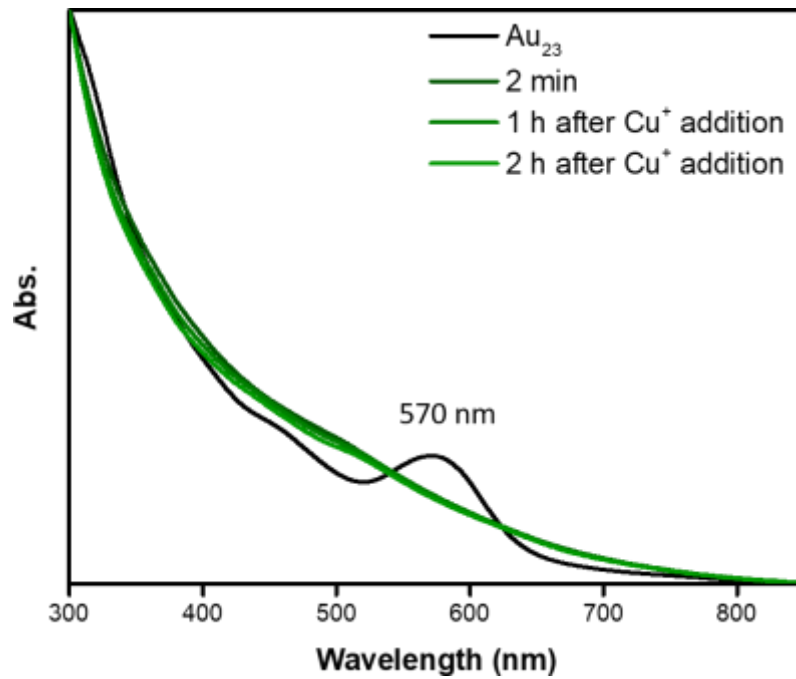


Figure S2. Time-dependent UV-vis absorption spectra during the transformation reaction of $[\text{Au}_{23}(\text{S-}i\text{-C}_6\text{H}_{11})_{16}]^- \text{NC}$.

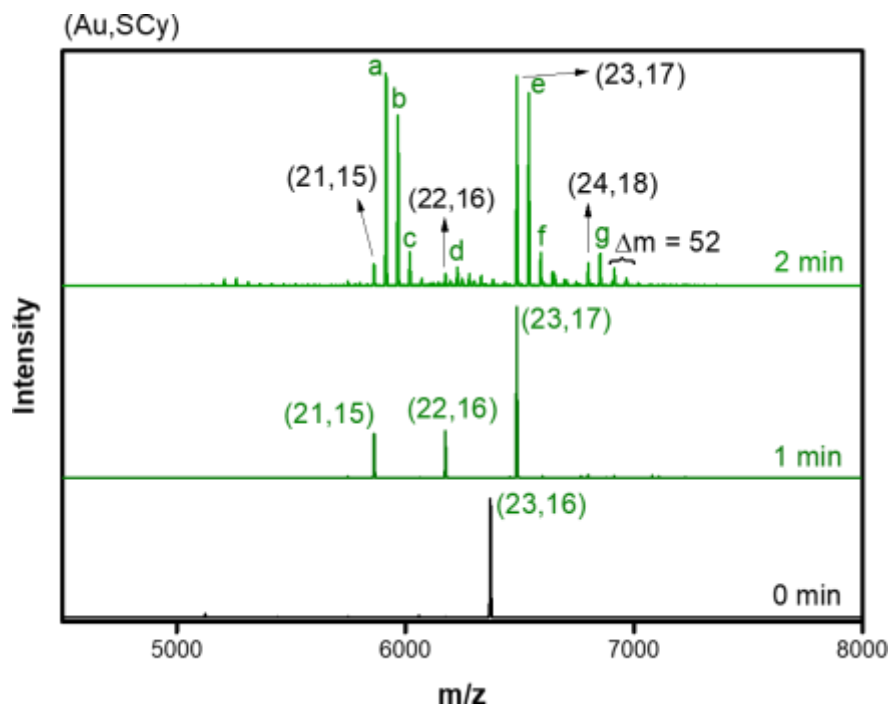


Figure S3. Time-dependent MALDI-TOF mass spectra during the transformation reaction of $[\text{Au}_{23}(\text{S-}c\text{-C}_6\text{H}_{11})_{16}]^-$ NC before the addition of Cu(I) salt.

Note: The peaks are labelled in such a way that the numbers in the bracket indicates the number of Au atoms and ligand molecules, respectively in each of the species, (SCy = S-*c*-C₆H₁₁).

Table S1. Table showing the formula and corresponding mass of the peaks from Fig. S3.

Peak	Formula	Observed Mass	Calculated Mass
a	$\text{Au}_{21}(\text{SCy})_{14}(\text{SAdm})_1$	5916.01	5916.61
b	$\text{Au}_{21}(\text{SCy})_{13}(\text{SAdm})_2$	5968.15	5968.69
c	$\text{Au}_{21}(\text{SCy})_{12}(\text{SAdm})_3$	6020.27	6020.76
d	$\text{Au}_{22}(\text{SCy})_{15}(\text{SAdm})_1$	6228.20	6228.79
e	$\text{Au}_{23}(\text{SCy})_{16}(\text{SAdm})_1$	6540.40	6540.98
f	$\text{Au}_{23}(\text{SCy})_{15}(\text{SAdm})_2$	6592.59	6593.05
g	$\text{Au}_{24}(\text{SCy})_{17}(\text{SAdm})_1$	6852.57	6853.16

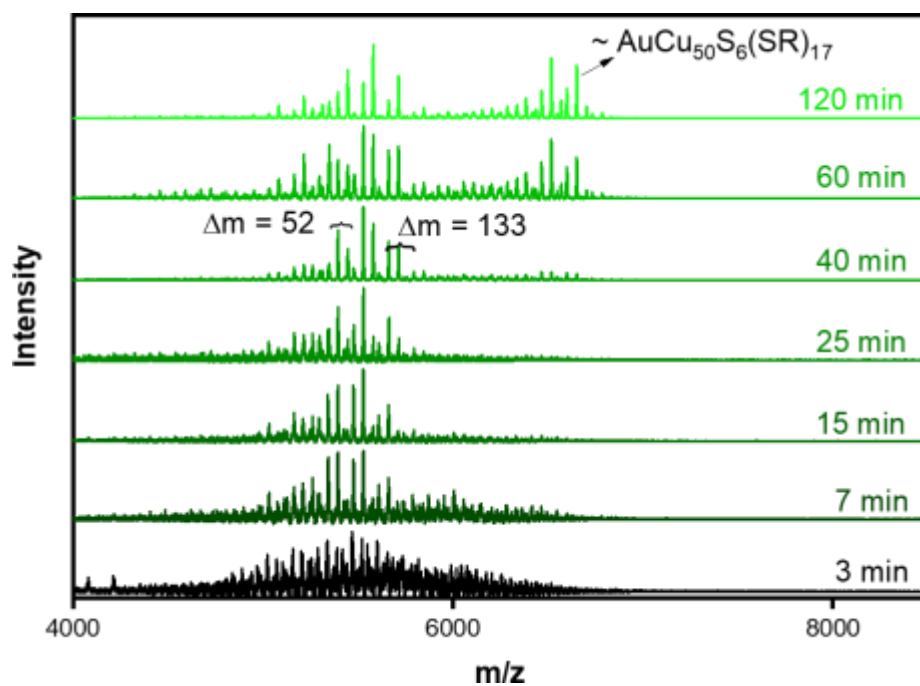


Figure S4. Time-dependent MALDI-TOF mass spectra during the transformation reaction of $[\text{Au}_{23}(\text{S-}c\text{-C}_6\text{H}_{11})_{16}]^-$ NC after the addition of Cu(I) salt.

Note: We were unable to identify the molecular-ion peak through mass spectrometry studies due to the severe fragmentation during ionization techniques and poor solubility of the NC.

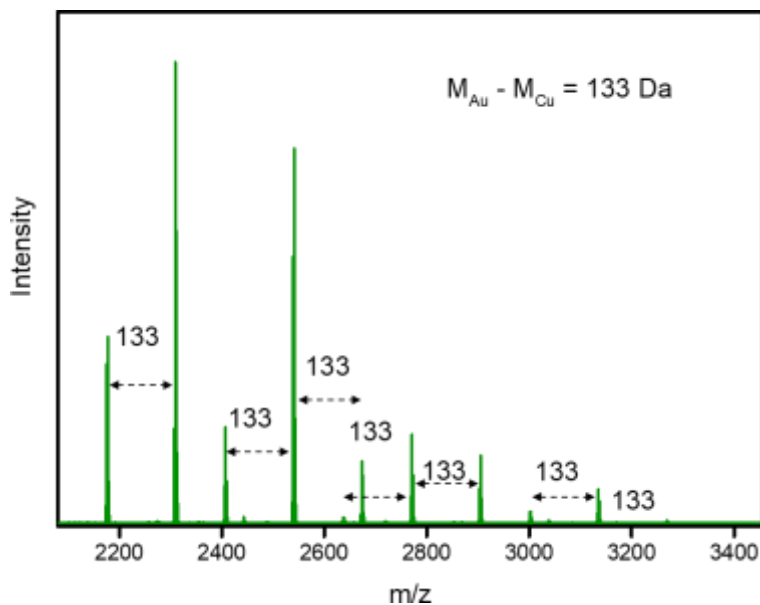


Figure S5. Positive-ion mode ESI mass spectrum of the aliquot taken during the transformation of $[\text{Au}_{23}(\text{S-}c\text{-C}_6\text{H}_{11})_{16}]^-$ NC.



Figure S6. Optical microscope images of the single crystals of $[\text{AuCu}_{56}\text{S}_{12}(\text{AdmS})_{20}(\text{O}_3\text{SAdm})_{12}]$ NC.

Table S2. Crystal structure refinement parameters of [AuCu₅₆S₁₂(AdmS)₂₀(O₃SAdm)₁₂] NC.

Identification code	0078_150424_sg53b
Empirical formula	C320 H480 Au1 Cu56 O36 S44
CCDC number	2426847
Formula weight	10068.86 g/mol
Temperature/K	100
Wavelength/Å	0.71073
Crystal system	Cubic
Space group	<i>Pa</i> -3 (No. 205)
<i>a</i> /Å	33.3470(4)
<i>b</i> /Å	33.3470(4)
<i>c</i> /Å	33.3470(4)
α /°	90
β /°	90
γ /°	90
Volume/Å ³	37082.6(13)
<i>Z</i>	4
$\rho_{\text{calc}}/\text{cm}^3$	1.804
μ/mm^{-1}	3.831
F(000)	20380.0
Crystal size/mm ³	0.160 × 0.150 × 0.130
2 θ range for data collection/°	3.664 to 56.582
Index ranges	-44 ≤ <i>h</i> ≤ 44, -40 ≤ <i>k</i> ≤ 42, -44 ≤ <i>l</i> ≤ 44
Reflections collected	226357
Independent reflections	15376 [<i>R</i> _{int} = 0.0868, <i>R</i> _{sigma} = 0.0428]
Data/restraints/parameters	15376/2070/1342
Goodness-of-fit on F ²	1.055
Final <i>R</i> indexes [<i>I</i> ≥ 2 σ (<i>I</i>)]	<i>R</i> ₁ = 0.0825, <i>wR</i> ₂ = 0.1909
Largest diff. peak/hole/ e Å ⁻³	1.01/-0.68

Table S3. Selected bond distances in [AuCu₅₆S₁₂(AdmS)₂₀(O₃SAdm)₁₂] NC.

Atoms	Bond length (Å)
Au(1) - Cu(10 ¹)	2.777(4)
Au(1) - Cu(10)	2.777(4)
Au(1) - Cu(20 ²)	2.804(8)
Au(1) - Cu(20 ³)	2.804(8)
Au(1) - Cu(20 ⁴)	2.804(8)
Au(1) - Cu(20 ⁵)	2.804(8)
Au(1) - Cu(15 ⁴)	2.788(9)
Au(1) - Cu(15 ²)	2.788(9)
Au(1) - Cu(15 ³)	2.788(9)
Au(1) - Cu(15 ⁵)	2.788(9)
Au(1) - Cu(15 ¹)	2.788(9)
Au(1) - Cu(15)	2.788(9)
Cu(3) - Cu(6)	2.583(3)
Cu(4) - Cu(5A)	1.498(4)
Cu(4) - Cu(17)	2.772(7)
Cu(6A) - Cu(8)	2.573(3)
Cu(4) - Cu(1 ⁷)	2.772(7)
Cu(6A) - Cu(8)	2.573(3)
Cu(6A) - Cu(7 ⁴)	1.504(4)
Cu(6A) - Cu(1A)	2.529(3)
Cu(5B) - Cu(8)	1.711(4)
Cu(5B) - Cu(7 ⁴)	1.363(5)
Cu(5B) - Cu(18 ⁴)	2.823(6)
Cu(2B) - Cu(8 ³)	1.502(4)
Cu(2B) - Cu(7 ⁵)	2.732(4)
Cu(4A) - Cu(3A)	1.786(7)
Cu(4A) - Cu(13)	2.774(7)
Cu(5) - Cu(2A)	1.438(4)
Cu(5) - Cu(8)	2.995(4)
Cu(6) - Cu(7)	2.602(5)
Cu(6) - Cu(14 ²)	2.959(9)
Cu(2A) - Cu(8 ³)	2.652(5)
Cu(8) - Cu(7 ⁴)	1.281(4)
Cu(8) - Cu(2 ⁵)	2.002(14)
Cu(8) - Cu(14)	2.762(7)
Cu(8) - Cu(18 ⁴)	2.775(5)
Cu(8) - Cu(21 ⁵)	2.862(9)
Cu(7) - Cu(5A ²)	2.717(4)
Cu(7) - Cu(14 ²)	2.922(8)
Cu(7) - Cu(12)	2.994(5)

Cu(7) - Cu(18)	2.638(5)
Cu(9) - Cu(1 ²)	2.017(9)
Cu(9) - Cu(1)	1.915(9)
Cu(9) - Cu(10)	2.911(4)
Cu(9) - Cu(11)	2.779(6)
Cu(5A) - Cu(17)	2.678(8)
Cu(3A) - Cu(13)	2.731(8)
Cu(14) - Cu(17)	2.321(13)
Cu(14) - Cu(17 ⁴)	2.840(11)
Cu(14) - Cu(17 ⁵)	2.669(14)
Cu(12) - Cu(10)	2.199(4)
Cu(12) - Cu(13 ²)	2.598(9)
Cu(12) - Cu(13)	2.547(9)
Cu(16) - Cu(15 ⁵)	2.092(14)
Cu(16) - Cu(15)	2.072(14)
Cu(10) - Cu(18 ²)	2.654(5)
Cu(10) - Cu(18)	2.654(5)
Cu(10) - Cu(18 ⁴)	2.654(5)
Cu(10) - Cu(11)	0.827(7)
Cu(10) - Cu(17)	2.683(8)
Cu(10) - Cu(17 ⁴)	2.683(8)
Cu(18) - Cu(20)	2.564(10)
Cu(18) - Cu(20 ²)	2.539(11)
Cu(18) - Cu(20 ³)	2.784(9)
Cu(21) - Cu(21 ⁵)	2.963(7)
Cu(21) - Cu((21 ³))	2.963(7)
Cu(11) - Cu(17)	2.892(10)

¹1-X,1-Y,1-Z; ²+Z,+X,+Y; ³1-Y,1-Z,1-X; ⁴+Y,+Z,+X; ⁵1-Z,1-X,1-Y

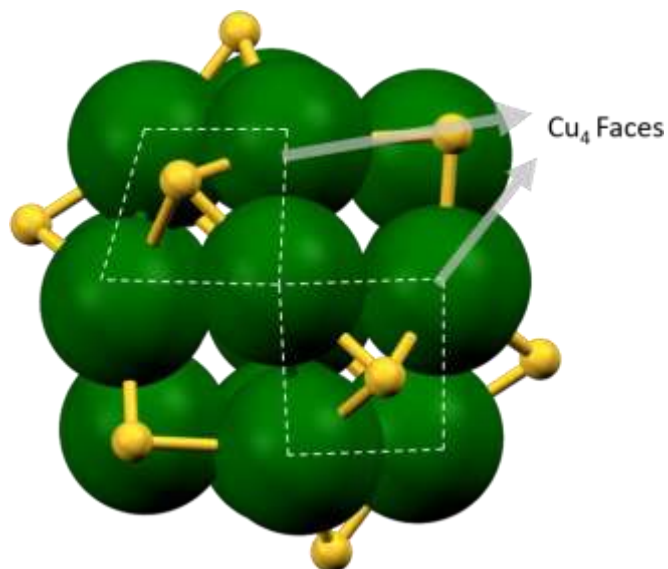


Figure S7. The innermost Cu_{14} rhombic dodecahedron shows the Cu_4 faces with μ^3 -bridging of sulphur on each face of the $[\text{AuCu}_{56}\text{S}_{12}(\text{AdmS})_{20}(\text{O}_3\text{SAdm})_{12}]$ NC. Color legend: green, Cu; yellow, S.

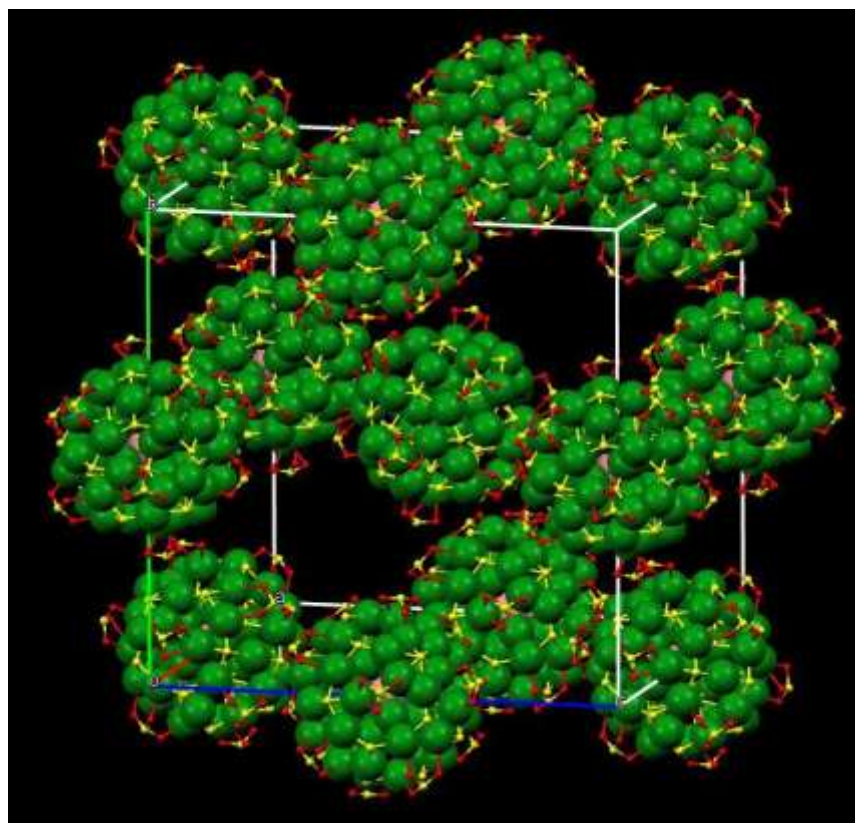


Figure S8. The unit cell packing of the $[\text{AuCu}_{56}\text{S}_{12}(\text{AdmS})_{20}(\text{O}_3\text{SAdm})_{12}]$ NC. Color legend: green, Cu; yellow, S; red, O.

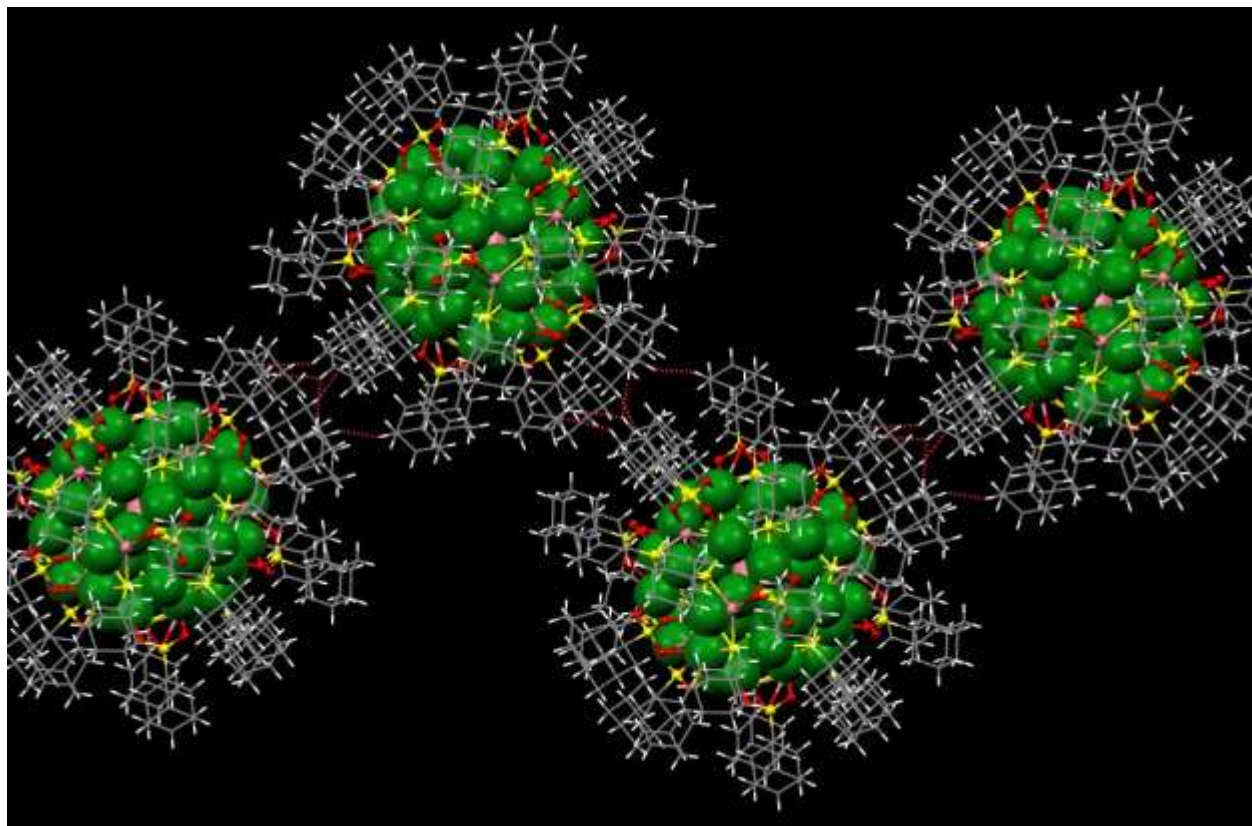
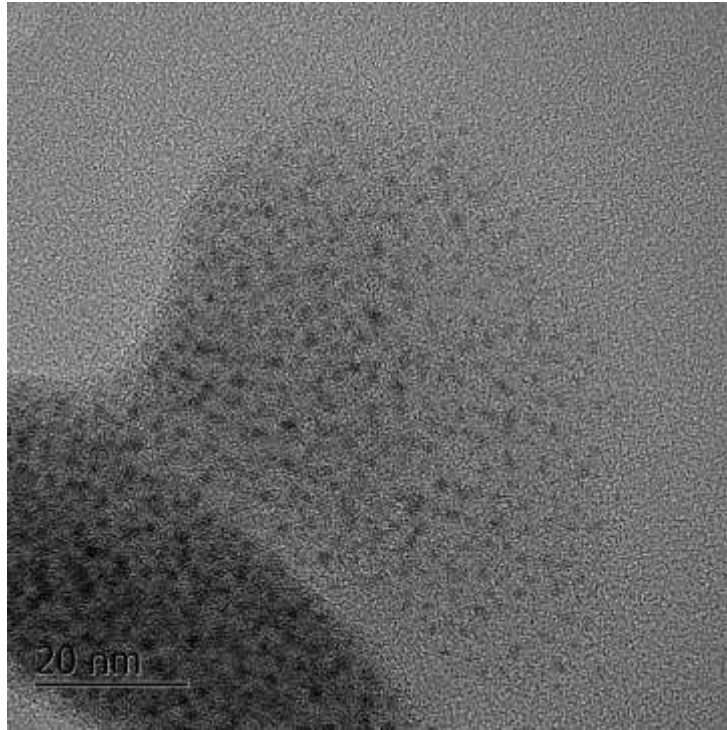


Figure S9. The intermolecular CH...HC non-bonding interactions directed the packing of the $[\text{AuCu}_{56}\text{S}_{12}(\text{AdmS})_{20}(\text{O}_3\text{SAdm})_{12}] \text{NC}$. Color legend: green, Cu; yellow, S; red, O.

a)



b)

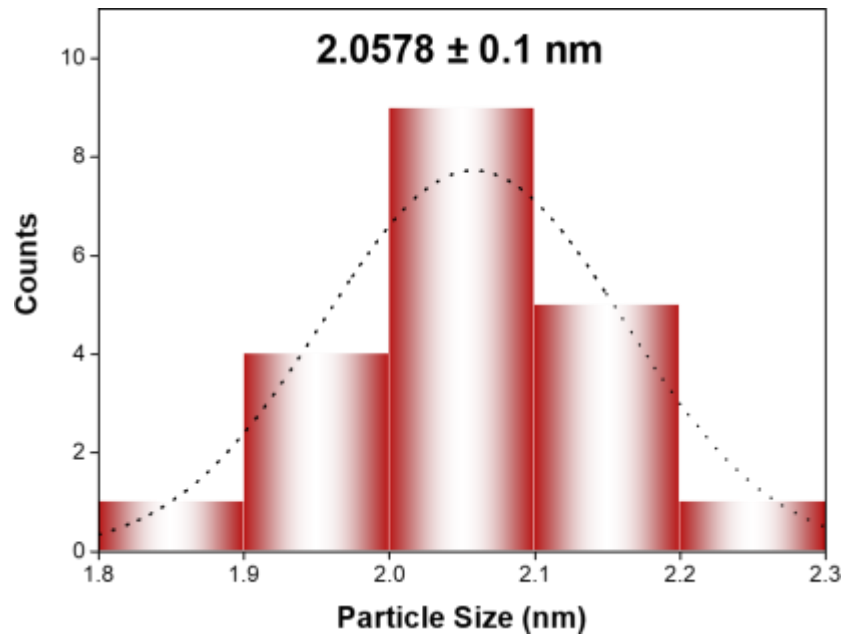


Figure S10. a) The TEM image showing the uniform distribution of the AuCu₅₆ NC and b) the bar diagram showing the average size of the particles.

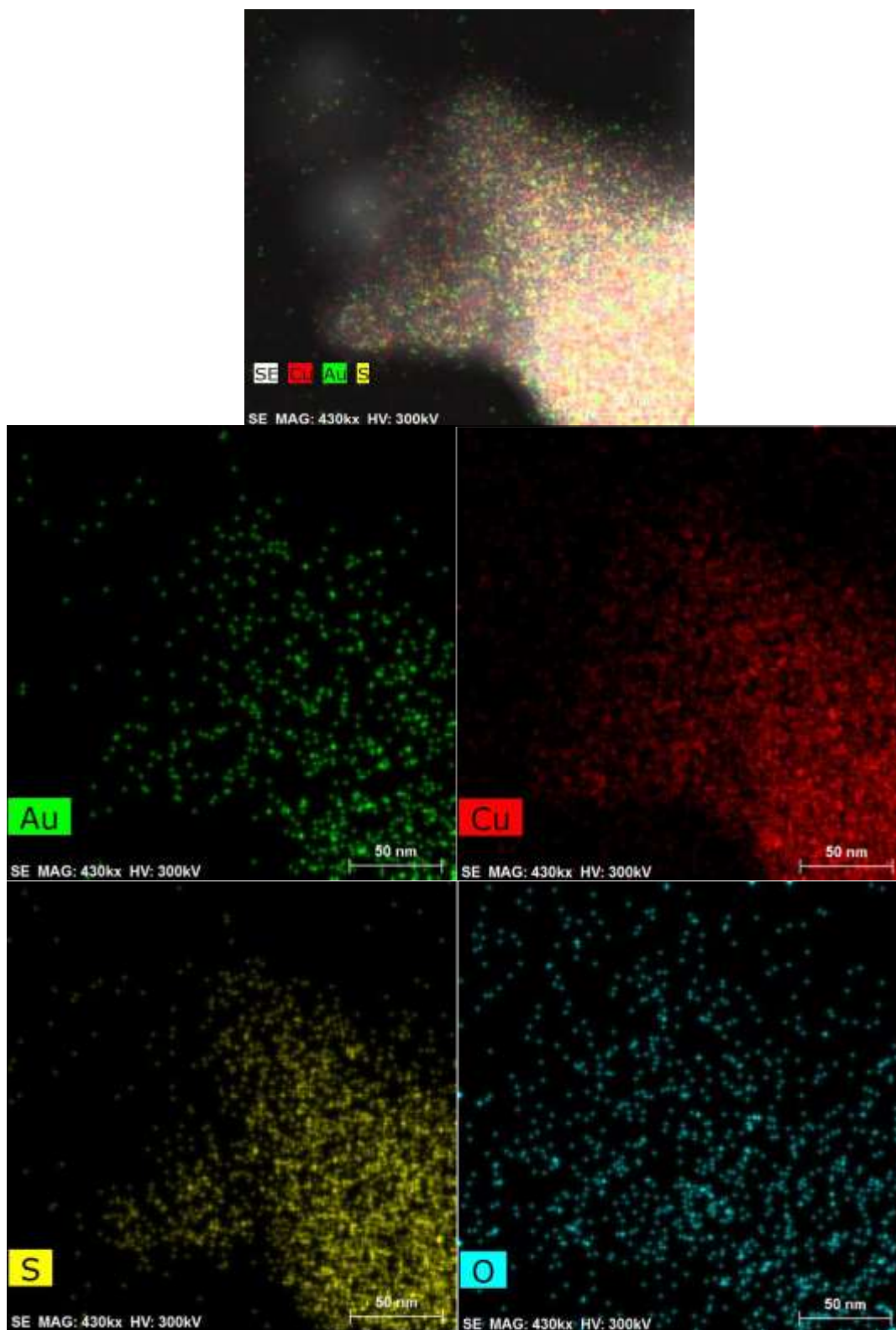


Figure S11. a) The TEM elemental analysis showing the presence of Au (green), Cu (red), S (yellow) and O (blue) in the AuCu₅₆ NC.

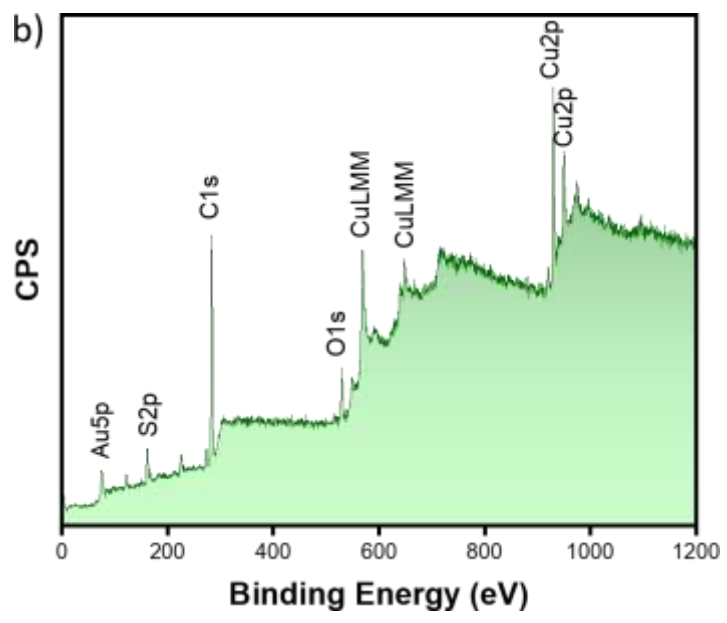
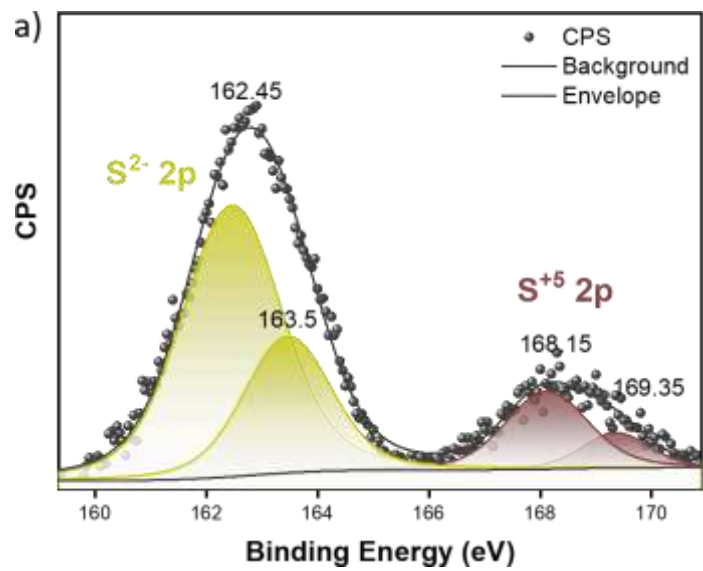


Figure S12. XPS spectra of the AuCu₅₆ NC showing a) the S 2p orbitals and b) the survey spectrum.

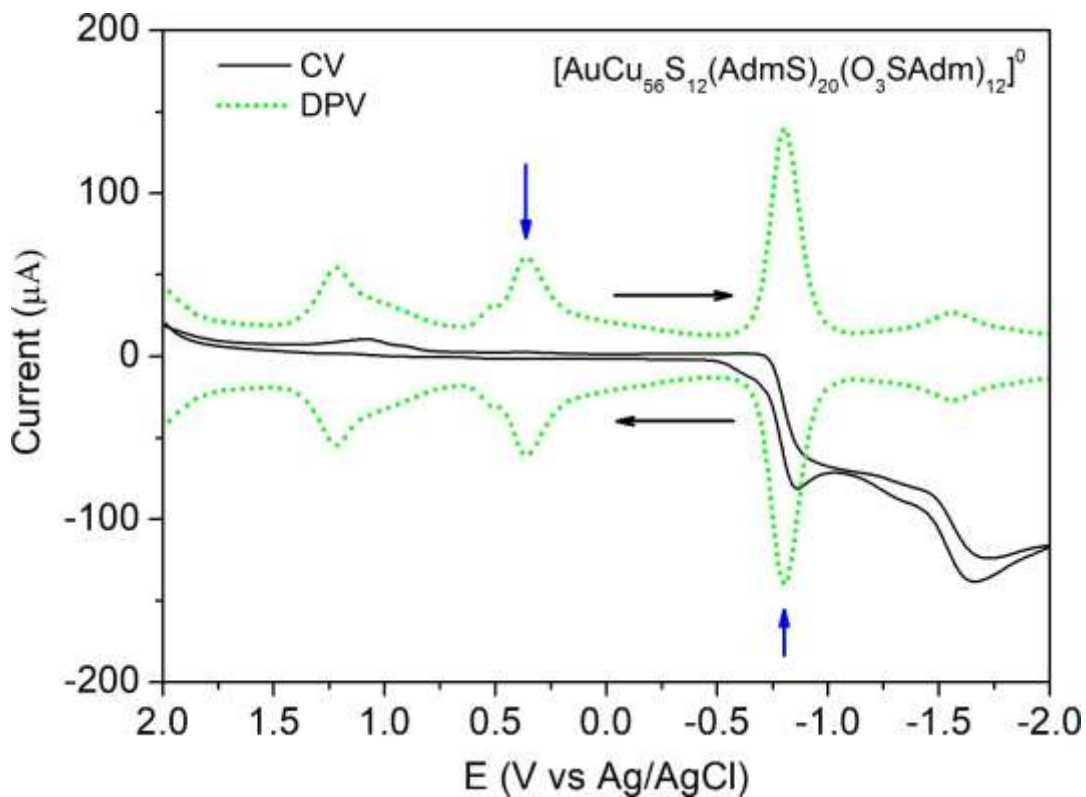


Figure S13. Cyclic (CVs) and differential pulse voltammograms (DPVs) of AuCu₅₆ NC at a GC electrode (15 mm). An electrolyte solution was prepared in MeCN with 0.1 M TBAPF₆ and degassed with N₂ for 20 min. The cyclic voltammetry (CV) was performed at a scan rate of 10 mV/s. For DPV measurements, a DC potential ramp of 10 mV/s and a pulse amplitude of 50 mV. The arrows indicate the first negative and positive voltammetric peaks.

Table S4. Experimental Formal Potential^a (V) differences (V) for synthesized NC in acetonitrile (MeCN) solvents containing 0.1 M NBu₄PF₆.

Solvent	Temperature	O1	O2	O3	O2-O1	O3-O2	R1	R2	R1-R2	O1-R1
CH ₃ CN	25 °C	0.37	0.5	1.22	0.13	0.72	-0.80	-1.5	0.70	1.17

^aFormal potentials (V) represent the mean values of the reduction and oxidation peak potentials observed during differential pulse voltammetry (DPV) scans (0.01 V/s)

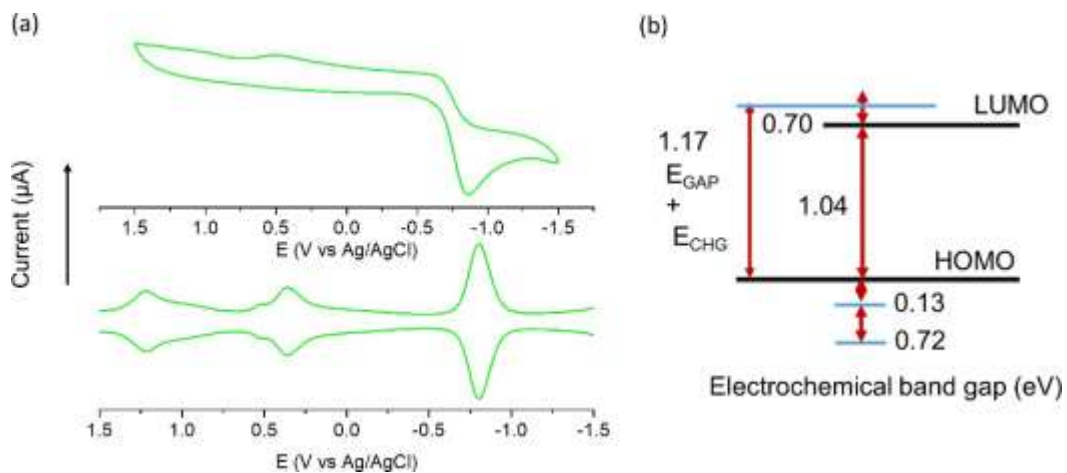


Figure S14. (a) Differential pulse voltammograms (DPVs) and cyclic voltammograms at 10 mV/s of AuCu₅₆ NC. Schematic representation of the energy level diagram for AuCu₅₆ NC based on data recorded in MeCN solution.

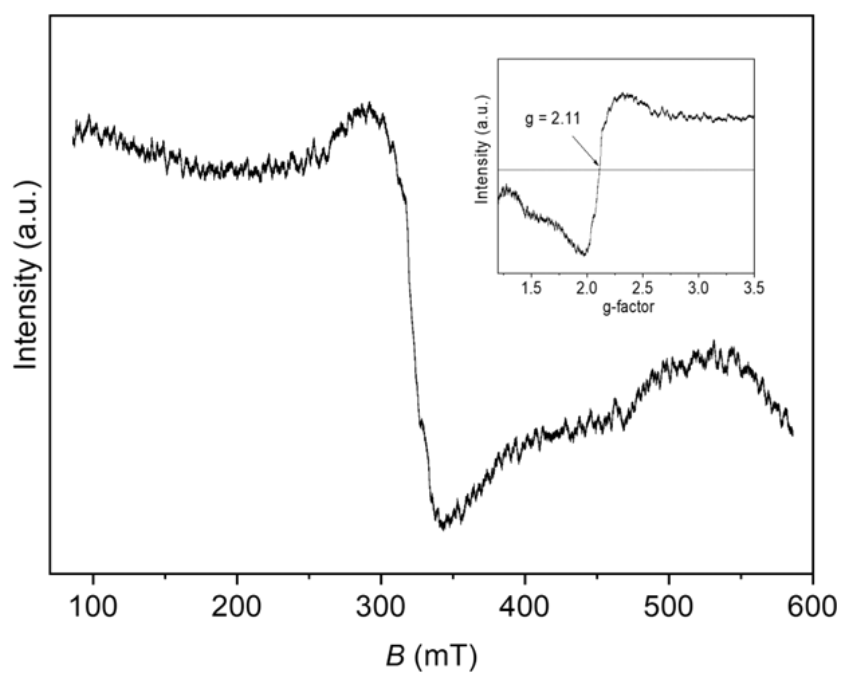


Figure S15. Electron Paramagnetic Resonance (EPR) spectrum of the AuCu₅₆ NC (solid sample) carried out at 298 K.

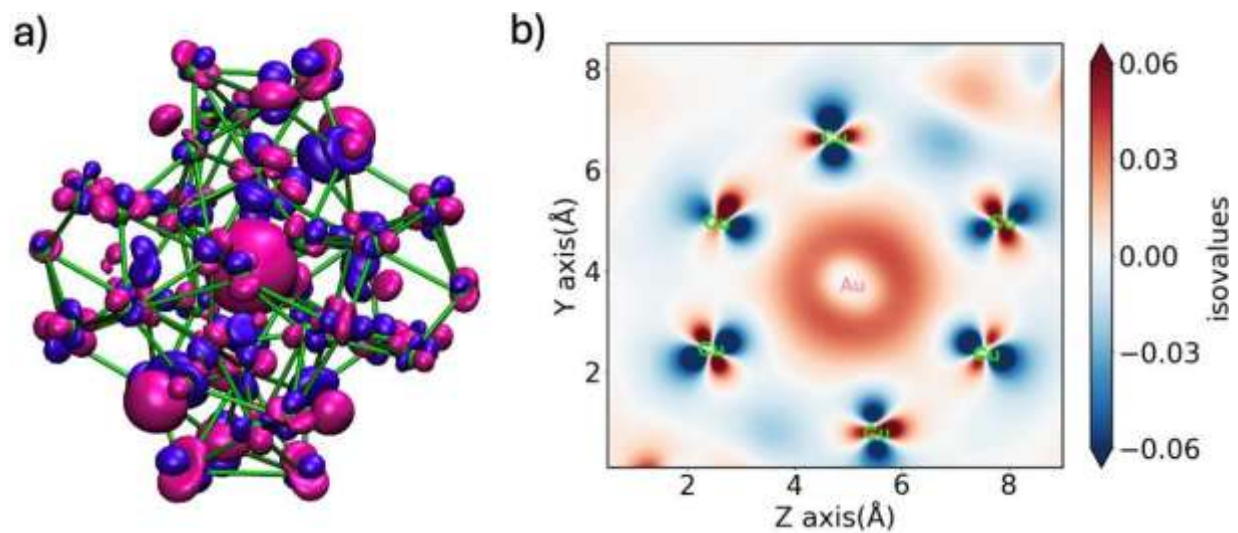


Figure S16. Concentric bond analysis of the core structure Au@Cu₁₄S₁₂@Cu₃₆ extracted from the optimized geometry of the AuCu₅₆ cluster: a) HOMO; b) contour plot of the HOMO projected along the 6-fold axis of the [Cu₁₄] rhombic dodecahedron.

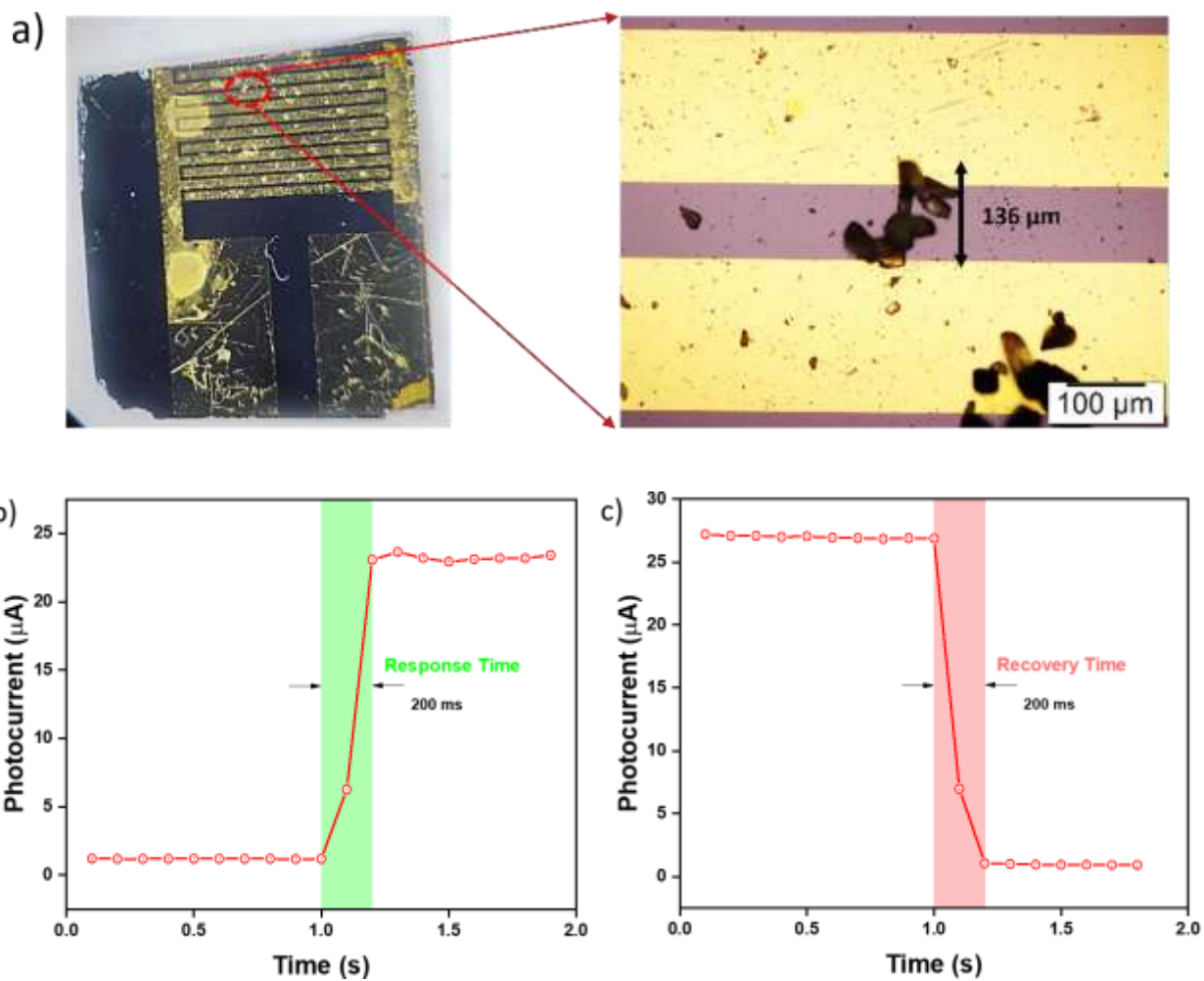


Figure S17. a) Optical microscopic image of the final device with AuCu₅₆ NC drop-casted on a prefabricated Interdigitated Electrodes (IDE) over Si/SiO₂ substrate with Cr/Au patterned electrodes for photocurrent measurements. b) Response time curve and c) recovery time of the device upon UV irradiation.

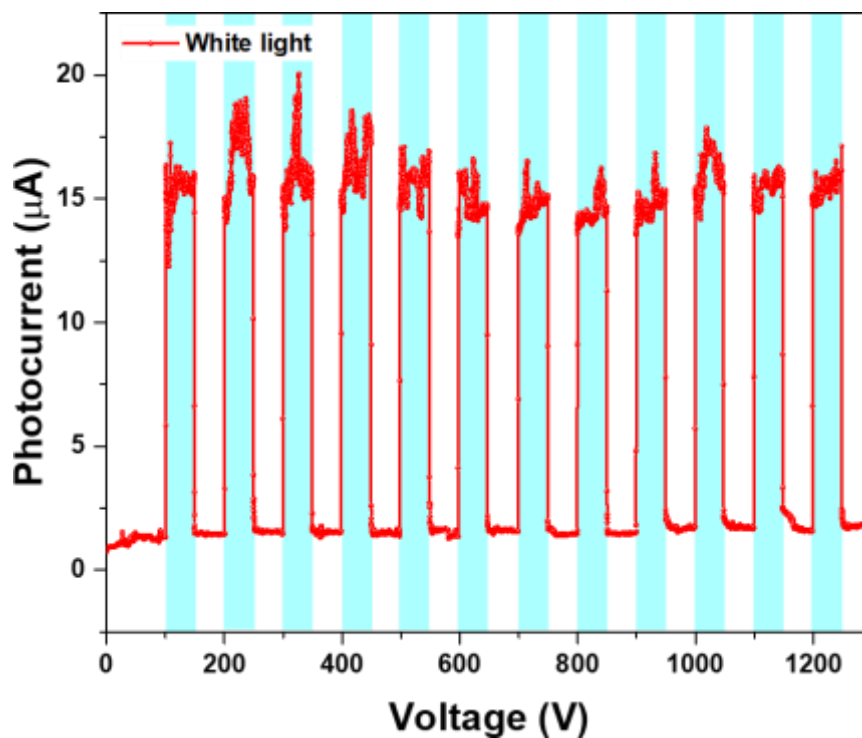


Figure S18. Photoresponse of the AuCu₅₆ NC drop-casted on a prefabricated Interdigitated Electrodes (IDE) under white light irradiation.

VI. References

- (S1) A. Das, T. Li, K. Nobusada, C. Zeng, N. L. Rosi and R. Jin, *J. Am. Chem. Soc.*, 2013, **135**, 18264–18267.
- (S2) L. Palatinus and G. Chapuis, *J. Appl. Crystallogr.*, 2007, **40**, 786–790.
- (S3) G. M. Sheldrick, *Acta Crystallogr. C Struct. Chem.*, 2015, **71**, 3–8.
- (S4) D. Kratzert, J. J. Holstein and I. Krossing, *J. Appl. Crystallogr.*, 2015, **48**, 933–938.
- (S5) O. V. Dolomanov, L. J. Bourhis, R. J. Gildea, J. A. K. Howard and H. Puschmann, *J. Appl. Crystallogr.*, 2009, **42**, 339–341.